Position Signal and Nonconduction Phase Current Based Fault Diagnosis Method of Position Sensor for Doubly Salient Electromagnetic Motor

Yijun Zhang, Bo Zhou, Wenjing Fang, Yi Lu, and Siyuan Jiang

***Abstract*—Reliable rotor position information is essential for accurate commutation control of motor drive system. Traditionally, hall sensors have been widely used to obtain rotor position information. The fault of position sensor will lead to the confusion of the commutation logic, which will reduce the output torque of the motor and even fail to operate normally. Therefore, fault diagnosis of position sensor is the key technology to improve the reliability of the system. In this article, a fault diagnosis method of position sensor is proposed for doubly salient electromagnetic motor (DSEM) drive system, which only needs the existing position signals, the driving signals of switch, and the nonconduction phase current. Compared with the existing method, the proposed method does not require additional hardware and complex calculation, can realize the fault diagnosis of single, two and three position sensors, and is not influenced by the variation of speed and load. Besides, the time of error commutation for the proposed method is less than 1/3 electrical angle period, which is helpful to switch the fault-tolerant strategy in time and minimize the damage to the system caused by the fault. In order to verify the effectiveness of the proposed method, experiments are carried out on a 12/8 pole DSEM equipped with three hall position sensors. The experimental results under both steady and dynamic conditions show that the proposed method can quickly realize fault location.**

***Index Terms*—Doubly salient electromagnetic motor (DSEM), fault diagnosis, nonconduction phase current, position sensor, position signal.**

NOMENCLATURE

H_{k} (k = 1,2,3)	Position signal of the position sensor k.
P_{m} (m = 1,2,3,4,5,6)	Driving signal of the switch $\mathrm{T_m}$.
i_{a},i_{b},i_{c}	Phase current.
$H_{\mathrm{k}}\uparrow$	Rising edge of H_{k}.
$H_{\mathrm{k}}\downarrow$	Falling edge of H_{k}.
$i_{\_\mathrm{nc}}$	Nonconduction phase current.
$F_{\_\mathrm{nc}}$	Judgment flag of $i_{\_\mathrm{nc}}$.
ε	Current threshold.
F_{det}, F_{ps}	Fault detection flag.
F_{k} (k = 1,2,3)	Fault location flag of position sensor k.
θ_{F}	Point of fault occurrence.
t_{err}	Time of error commutation.

Manuscript received 19 November 2023; revised 20 February 2024; accepted 4 April 2024. Date of publication 10 April 2024; date of current version 16 May 2024. This work was supported by the Key Project of National Natural Science Foundation of China under Grant 51737006. Recommended for publication by Associate Editor J. Hur. *(Corresponding author: Bo Zhou.)*

Yijun Zhang, Bo Zhou, Wenjing Fang, and Yi Lu are with the Colleague of Automation Engineering, Nanjing University of Aeronautics and Astronautics, Nanjing 210016, China (e-mail: yijunzhang@nuaa.edu.cn; zhoubo@nuaa.edu.cn; wjfang@nuaa.edu.cn; bx2103502@nuaa.edu.cn).

Siyuan Jiang is with the School of Electrical Engineering and Automation, Henan Polytechnic University, Jiaozuo 454003, China (e-mail: jsy@hpu.edu.cn).

Color versions of one or more figures in this article are available at https://doi.org/10.1109/TPEL.2024.3386983.

Digital Object Identifier 10.1109/TPEL.2024.3386983

I. INTRODUCTION

AS A new type of brushless dc motor, doubly salient electromagnetic motor (DSEM) has the advantages of simple structure, flexible magnetic field adjustment, and high reliability, which has a good application prospect in the fields of aviation and electric vehicles [1], [2], [3], [4], [5]. The brushless motor needs to control the turn-on sequence of each phase and turn-on time of each phase through the position sensor to achieve accurate control of output torque. The correct position signal processing can ensure that the motor is commutated in the correct position, which makes the motor run according to the predetermined target [6], [7]. Therefore, the position signal is very important.

Three position sensors are usually used to acquire position signal in motor drive system. However, position sensors may fail in actual operation due to various reasons, such as harsh environment and vibration [8], [9], [10]. The fault of position sensor will lead to the confusion of the commutation logic in motor drive system, which will reduce the output torque of the motor and even fail to operate normally [11]. Therefore, in order to improve the reliability of the DSEM drive system, it is necessary to develop fault diagnosis of position sensor.

So far, research on fault diagnosis of position sensor for DSEM is still in the early stage on which only one literature was retrieved. Method proposed in [12] is based on the rising edge variation of the position signal, and although this method achieves fault diagnosis of position sensor, there are some limitations.

1) The time threshold is introduced, which is only applicable to steady conditions. When the motor is running under dynamic conditions, such as acceleration, deceleration, loading, and load reduction, this method will cause misdiagnosis.
2) The diagnostic range is limited. The method is based on the alternating variation sequence of the rising edge for the position signal, which makes it difficult to distinguish the

fault of single and two position sensors at the same time. When the three position sensors are faulty, the position signal cannot generate the rising edge and the method will fail.

3) The maximum value for the time of error commutation (i.e., the continuous output time of negative torque) is 1/3 electrical angle period, which is not be beneficial for the operation of the motor.

In summary, it is necessary to solve above three problems to realize fault diagnosis of position sensor. Since the inductance characteristics of DSEM are similar to switched reluctance motor (SRM), and back electromotive force (EMF) of DSEM is similar to brushless dc motor (BLDCM), the fault diagnosis methods of position sensor for SRM and BLDCM are of great reference significance for solving the above three problems, which exist in fault diagnosis of position sensor for DSEM.

For SRM, methods proposed in [13] and [14] are based on the detection of edge trigger sequence for position signal and the calculation of angle difference of adjacent edges. A fault diagnosis method based on the synthetic hybrid-integral threshold logic is proposed for SRM drives [15]. The above methods can only diagnose single position sensor fault. Besides, the above methods all assume that the angular velocity of the rotor on the adjacent edge is constant. However, when the motor is accelerating or decelerating, this assumption is not valid. In order to solve this problem, a diagnosis method based on the edge time prediction is proposed in [16], which assumed that the angular acceleration of adjacent edge was constant. This method could be applied to constant speed and the variation of uniform speed, but could not be applied to the variation of nonuniform speed. In summary, methods proposed in [13], [14], [15], and [16] also have the same problems as fault diagnosis of position sensor in DSEM, so the above methods cannot be directly applied to DSEM.

For BLDCM, method proposed in [17] can realize fault location by generating additional position information based on the redundant position sensor. This method is not influenced by the variation of speed and load, and can diagnose the fault of single and multiple position sensors. However, this method increases the diagnosis cost. In order to solve this problem, a fast fault diagnosis method is proposed, which can realize the fault diagnosis of single and two position sensors [18]. However, the proposed method depends on the time threshold τ, and may cause misdiagnosis once the speed and load vary. A combined circuit for detecting hall position sensor faults is proposed in [19], which relies only on three position signals to achieve fault diagnosis of position sensor. However, this method is only applicable to fault diagnosis of single position sensor and the time of error commutation is 1/3 electrical angle period. In summary, Zhang and Feng [18] and Mousmi et al. [19] cannot simultaneously solve the above three problems, which exist in fault diagnosis of position sensor in DSEM, while [17] requires three additional position sensors, which increases the diagnosis cost.

Based on the aforementioned methods and combining the back EMF variation characteristic of DSEM, a fault diagnosis method of position sensor is proposed in this article. First, the position signals and the variation characteristics of the phase currents under different chopping modes are analyzed after the position sensor fault. Second, in order to reduce the time of error commutation, a fault diagnosis method of single, two and three position sensors are proposed based on the existing position signal, the driving signal of switch and the nonconduction phase current under chopping lower switch control. The proposed method can solve three problems existing in the fault diagnosis of DSEM position sensors without increasing the diagnosis cost, which is the main contribution of this article. Finally, in order to verify the effectiveness of the proposed method, experiments are carried out on a 12/8 pole DSEM equipped with three position sensors.

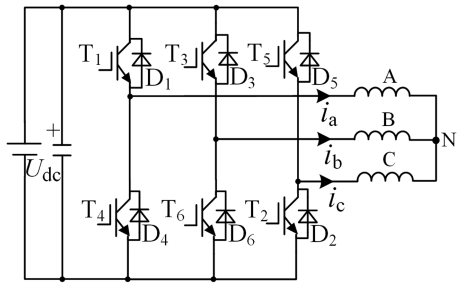

Fig. 1 Inverter topology of DSEM.

The rest of this article is organized as follows. The working principle of DSEM and fault analysis of position sensor are introduced in Section II. The proposed fault diagnosis method is detailed in Section III. The fault experimental results are shown in Section IV. Finally, Section V concludes this article.

II. Working Principle of DSEM and Fault Analysis of Position Sensor

A. Working Principle of DSEM

Fig. 1 shows the inverter topology of DSEM, where $U_{\rm dc}$ is the dc bus voltage; A, B, and C are the armature windings; $i_{\rm p}$ (p = a, b, c) is the phase current, whose positive direction is shown in Fig. 1.

Fig. 2 shows the position signal, phase current and conduction logic of switch under normal operation of motor, where $L_{\rm p}$ is the self-inductance of the armature winding; $L_{\rm pf}$ is the mutual inductance between the armature winding and the excitation winding; $H_{\rm k}$ (k = 1, 2, 3) is the position signal of the position sensor k; θ is the rotor position angle. When the motor is running normally, the DSP enters the capture interrupt by capturing $H_{\rm k}\uparrow$ ($H_{\rm k}\uparrow$ represents the rising edge of $H_{\rm k}$) and gives the commutation information. Taking 0°–360° (one electrical angle period) as an example, $H_1\uparrow$ appears at 0° and $\rm T_1T_2$ works in the 0°–120° interval; $H_2\uparrow$ appears at 120° and $\rm T_3T_4$ works in the 120°–240° interval; $H_3\uparrow$ appears at 240° and $\rm T_5T_6$ works in the 240°–360° interval. For the convenience of description, 0°–120°, 120°–240°, and 240°–360° were defined as sector 1, sector 2, and sector 3, respectively.

$$P_{\rm m} = \begin{cases} 1 & \text{switch } \rm T_m \text{ on} \\ 0 & \text{switch } \rm T_m \text{ off} \end{cases}. \tag{1}$$

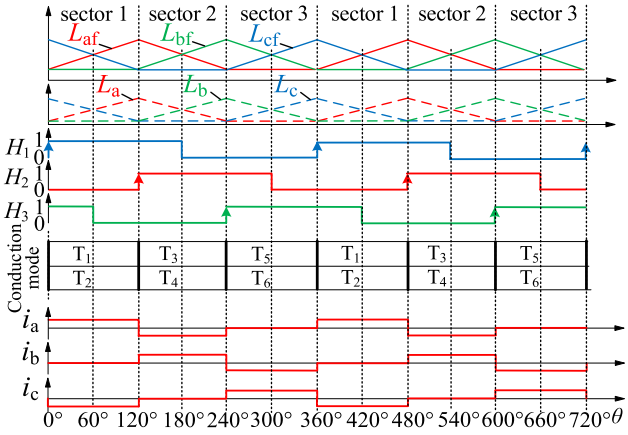

Fig. 2 Position signal, phase current, and conduction logic of switch under normal operation of the motor.

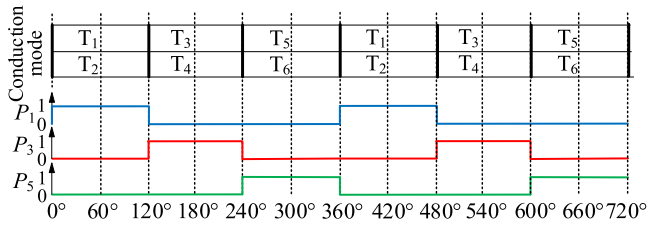

Fig. 3 Driving signals of upper switch under the mode of chopping lower switch.

The P_m (m = 1, 2, 3, 4, 5, 6) defined in (1) is the driving signal of the switch T_m. The chopper mode of T_m has two ways: chopping double switch and chopping single switch. Since the switch loss under the mode of chopping double switch is greater than that under the mode of chopping single switch, the mode of chopping single switch is usually adopted. The mode of chopping single switch includes chopping upper switch control and chopping lower switch control. Taking chopping lower switch control as an example, the upper switch working in each sector maintains the state of continuous on, as shown in Fig. 3. For example, P_1 is always 1 in the 0°–120° interval, corresponding to the upper switch T_1 is continuously on.

B. Fault Analysis of Position Sensor

After the fault of position sensor, there are two cases: $H_k \equiv 1$ and $H_k \equiv 0$. According to the difference of H_k before and after the fault, the fault performance of position sensor has the following four types: 1) H_k is 0 before and after the fault, defined low level fault 1; 2) H_k before the fault is 1 and after the fault is 0, defined low level fault 2; 3) H_k is 1 before and after the fault, defined high level fault 1; 4) H_k before the fault is 0 and after the fault is 1, defined high level fault 2.

Taking the fault of position sensor 1 as an example, the four fault performances are shown in Fig. 4, where t_{err} is the time of error commutation. Taking Fig. 4(a) as an example and comparing Fig. 2, the influence of position sensor fault on the system can be obtained: $H_1\uparrow$ is generated at 360° in Fig. 2, which

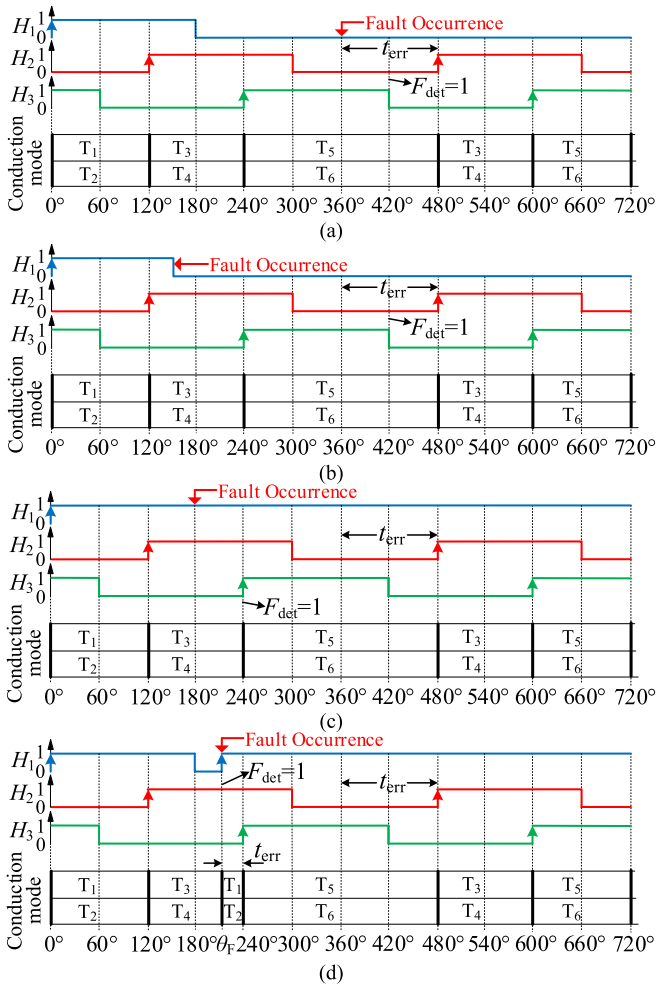

Fig. 4 Fault performance of position sensor 1. (a) Low level fault 1. (b) Low level fault 2. (c) High level fault 1. (d) High level fault 2.

makes T_5T_6 work switched to T_1T_2 work. However, $H_1\uparrow$ cannot be generated at 360° in Fig. 4(a) and commutation cannot be achieved, which makes T_5T_6 continue to work in the 360°–480° interval, and t_{err} is 1/3 electrical angle period.

It can be seen from Fig. 4 that H_1 is always 1 or 0 after fault, and the rising edge of H_1 cannot be generated again, which makes it impossible to realize the correct commutation. Therefore, the fault position should be detected in time and fault-tolerant control should be carried out.

III. Proposed Fault Diagnosis Method

A. Fault Detection

When the position sensor is normal, it can be seen from Fig. 2 that six jumping edges are generated by H_k in an electrical angle period (taking 0°–360° interval as an example): 1) $H_1\uparrow$, $H_2 = 0$, and $H_3 = 1$ at $\theta = 0°$ or 360°, which means $H_1 \uparrow \cap \overline{H_2} \cap H_3 = 1$, where $\overline{H_k}$ denotes inverse operation H_k; 2) $H_1 \cap \overline{H_2} \cap H_3 \downarrow = 1$ at $\theta = 60°$, where $H_k\downarrow$ denotes the falling edge of H_k; 3) $H_1 \cap H_2 \uparrow \cap \overline{H_3} = 1$ at $\theta = 120°$; 4) $H_1 \downarrow \cap H_2 \cap \overline{H_3} = 1$ at $\theta = 180°$; 5) $\overline{H_1} \cap H_2 \cap H_3 \uparrow = 1$ at $\theta = 240°$; 6) $\overline{H_1} \cap H_2 \downarrow$

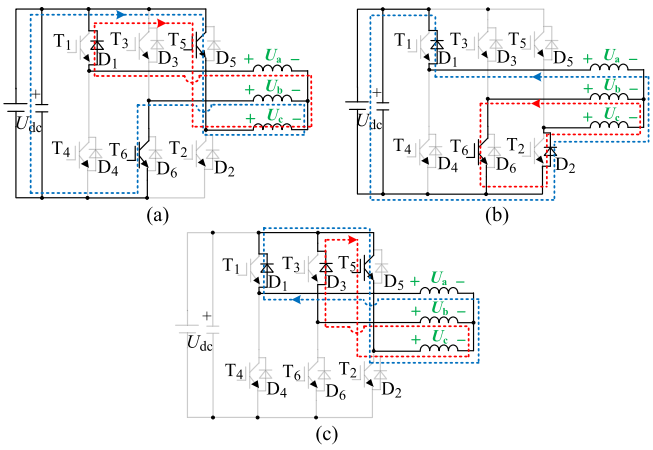

Fig. 5 Current loops of the 360°–420° interval in Fig. 4(a) under the chopping single switch control mode. (a) T_5T_6 ON. (b) T_5 OFF T_6 ON. (c) T_5 ON T_6 OFF.

$\cap H_3 = 1$ at $\theta = 300°$. When the position sensor k fails, it can be seen from the analysis of B in Section II that H_k is always 1 or 0, and the jumping edge of H_k cannot be generated again, which makes it impossible for H_k to satisfy simultaneously 1)–6) above. Therefore, once H_k does not meet the above 1)–6), it indicates that the position sensor is faulty, as shown in (2) shown at the bottom of the page, where $F_{det} = 1$ indicates that the position sensor is faulty and $F_{det} = 0$ indicates that the sensor is normal.

However, fault detection by $F_{det} = 1$ may make the time of error commutation too long. As shown in Fig. 4(a), $F_{det} = 1$ cannot be detected at 360° and can only be detected at 420°. Therefore, in order to reduce the time of error commutation, it is necessary to achieve fault detection between 360° and 420° in Fig. 4(a) as far as possible. Since two phase windings work in each sector of DSEM, the current generated in the third phase winding is set to the nonconduction phase current $i_{\_nc}$. When the position sensor is normal, it can be seen from Fig. 2 that $i_{\_nc} = i_b = 0$ when T_1T_2 works, $i_{\_nc} = i_c = 0$ when T_3T_4 works, and $i_{\_nc} = i_a = 0$ when T_5T_6 works. When position sensor 1 is faulty, it can be seen from Fig. 4(a) that T_5T_6 works in 360°–420° interval. In order to find fault detection characteristics, it is analyzed below whether $i_{\_nc}$ (i.e., i_a) is still 0 for T_5T_6 operation. If not, fault detection can be realized.

1) If chopping upper switch control is adopted, the two operating states of T_5T_6 during the 360°–420° interval in Fig. 4(a) are T_5T_6 ON and T_5 OFF T_6 ON, respectively.

When T_5T_6 is ON, the phase winding A and phase winding C form a current loop with the bus voltage U_{dc}, as shown in the blue loop in Fig. 5(a), where U_p is the voltage of phase winding. Besides, D_1 is on due to the effect of the back EMF and a current loop is formed, as shown in the red loop in Fig. 5(a). It can be seen from Fig. 5(a) that i_a will decrease from 0.

When T_5 is OFF and T_6 is ON, the phase winding B forms a current loop with phase winding C through T_6 and D_2, as shown in the red loop in Fig. 5(b). Meanwhile, phase winding A forms a current loop with the phase winding C through D_1, U_{dc} and D_2, as shown in the blue loop in Fig. 5(b). According to the Kirchhoff's voltage law (KVL), the loop voltage equation in Fig. 5(b) can be obtained as follows:

$$\begin{cases} U_{dc} = U_a - U_c; U_b = U_c \\ U_p = i_p R + L_p di_p/dt + e_p \\ e_p = i_p \omega dL_p/d\theta + i_f \omega dL_{pf}/d\theta \end{cases} \tag{3}$$

where e_p is the back EMF, R is the internal resistance of armature winding, and ω is the rotor angular speed. Since $dL_p/d\theta$ is much smaller than $dL_{pf}/d\theta$, e_p is approximately equal to $i_f \omega dL_{pf}/d\theta$ [20]. Besides, since the $i_p R$ is very small compared to U_{dc}, it is ignored. Finally, substituting $i_a + i_b + i_c = 0$ into (3) to obtain the variation rate of i_a as follows:

$$\frac{di_a}{dt} = \frac{L_b (U_{dc} - e_a + e_c) + L_c (U_{dc} - e_a + e_b)}{L_a L_b + L_a L_c + L_b L_c} \tag{4}$$

according to $dL_{af}/d\theta > 0$, $dL_{bf}/d\theta = 0$, and $dL_{cf}/d\theta < 0$ during the 360°–420° interval in Fig. 2, it can be obtained that $e_a > 0$, $e_b = 0$ and $e_c < 0$ in (4). Meanwhile, according to $U_{dc}/2 > e_p$ [21], it can be obtained that the variation rate of i_a in (4) is greater than 0, i.e., i_a increases to 0.

2) If chopping lower switch control is adopted, the two operating states of T_5T_6 during the 360°–420° interval in Fig. 4(a) are T_5T_6 ON and T_5 ON T_6 OFF, respectively.

When T_5T_6 is ON, the current loop is the same as Fig. 5(a), i.e., i_a decreases from 0.

When T_5 is ON and T_6 is OFF, the phase winding B forms a current loop with phase winding C through D_3 and T_5, as shown in the red loop in Fig. 5(c). Meanwhile, the phase winding A forms a current loop with phase winding C through D_1 and T_5, as shown in the blue loop in Fig. 5(c). According to the KVL, the loop voltage equation in Fig. 5(c) can be obtained as follows:

$$\begin{cases} U_a = U_c; U_b = U_c \\ U_p = i_p R + L_p di_p/dt + e_p \\ e_p = i_p \omega dL_p/d\theta + i_f \omega dL_{pf}/d\theta. \end{cases} \tag{5}$$

A similar solution to (4) is used to obtain the variation rate of i_a in (5) as follows:

$$\frac{di_a}{dt} = \frac{L_b (e_c - e_a) + L_c (e_b - e_a)}{L_a L_b + L_a L_c + L_b L_c}. \tag{6}$$

According to $dL_{af}/d\theta > 0$, $dL_{bf}/d\theta = 0$, and $dL_{cf}/d\theta < 0$ during the 360°–420° interval in Fig. 2, it can be obtained that $e_a > 0$,

$$\begin{cases} \text{if} \begin{pmatrix} H_k \uparrow \textbf{or} \\ H_k \downarrow \\ \text{appears} \end{pmatrix}, F_{det} = \begin{bmatrix} (\overline{H_1 \uparrow \cap \overline{H_2} \cap H_3}) \cup (\overline{H_1 \cap \overline{H_2} \cap H_3 \downarrow}) \cup \\ (\overline{H_1 \cap H_2 \uparrow \cap \overline{H_3}}) \cup (\overline{H_1 \downarrow \cap H_2 \cap \overline{H_3}}) \cup \\ (\overline{H_1} \cap H_2 \cap H_3 \uparrow) \cup (\overline{H_1} \cap H_2 \downarrow \cap H_3) \end{bmatrix} \\ \text{otherswise}, \quad F_{det} = 0 \end{cases} \tag{2}$$

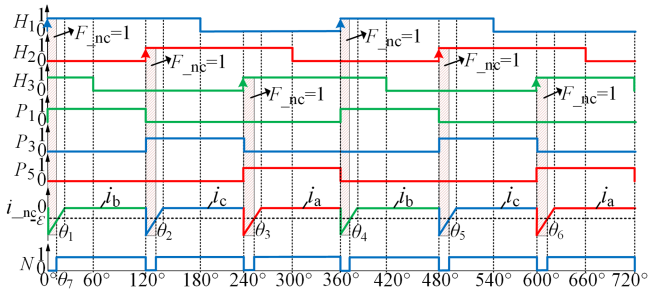

Fig. 6 Nonconduction phase current $i_{\_nc}$ of the motor in normal operation under chopping lower switch control.

$e_b = 0$, and $e_c < 0$ in (6) and the variation rate of i_a is less than 0, i.e., i_a decreases.

In summary, the characteristics of i_a in the 360°–420° interval of Fig. 4(a) are as follows: if chopping upper switch control is adopted, i_a will not continue to decrease from 0; if chopping lower switch control is adopted, i_a decreases continuously from 0. Therefore, the obvious characteristics of fault detection can be obtained by adopting chopper lower switch control, i.e., $i_{\_nc} = i_a \neq 0$. The $i_{\_nc}$ judgment flag $F_{\_nc}$ is defined as follows:

$$F_{\_nc} = \begin{cases} 1 & i_{\_nc} \le -\varepsilon \\ 0 & \text{others} \end{cases} \tag{7}$$

where $F_{\_nc} = 1$ indicates that a fault occurs, otherwise the system is normal; ε indicates the current threshold. In order to prevent misdiagnosis, ε should be greater than the maximum value of sampling error when $i_p = 0$. In order to prevent missing diagnosis, ε should be less than the current amplitude of motor no-load running.

It is noted that the waveforms of phase currents in Fig. 2 are ideal cases, while commutation process is existed during the actual operation of the motor, as shown in Fig. 6, where 0°–θ_1, 120°–θ_2, 240°–θ_3, 360°–θ_4, 480°–θ_5, and 600°–θ_6 are all commutation intervals. It can be seen that $i_{\_nc} \le -\varepsilon$ in the shaded part of the commutation interval, and $F_{\_nc} = 1$ is obtained by combining (7), which generated a misdiagnosis. Since the misdiagnosis occurs only in the shaded part of Fig. 6, the misdiagnosis problem can be solved if the fault diagnosis is performed outside the shaded part. Therefore, the key to eliminating the misdiagnosis problem is to determine the start and end of the shaded part in Fig. 6.

Since the start and end of the shadow part in Fig. 6 correspond to the rising edge of the driving signal of upper switch (P_1, P_3, P_5) and the nonconduction phase current $i_{\_nc} = -\varepsilon$, respectively, the rising edge of the upper switch drive signal and $i_{\_nc} = -\varepsilon$ can be used as the mark of the start and end of the shaded part, respectively. Based on the above, variable N is introduced and its value is determined, as shown in Fig. 7. Taking the 0°–120° interval of Fig. 6 as an example, the variation characteristics of N are analyzed combined with Fig. 7: 1) When $\theta = 0°$, due to the rising edge of P_1, $N = 0$ can be obtained by Fig. 7; 2) When $0° < \theta < \theta_7$ (θ_7 is the position angle at which $i_{\_nc} = -\varepsilon$), due to $i_{\_nc} < -\varepsilon$, N is still 0 by Fig. 7; 3) When $\theta = \theta_7$, due to $i_{\_nc} = -\varepsilon$, N jumps from 0 to 1 by Fig. 7; 4) When $\theta_7 < \theta <$ 120°, since there is no rising edge of the driving signal of upper switch, N is still 1 by Fig. 7; 5) When $\theta = 120°$, due to the rising edge of P_3, N jumps from 1 to 0 by Fig. 7. The analysis of N in other intervals is similar to that in the 0°–120° interval, and the waveform of N is obtained, as shown in Fig. 6.

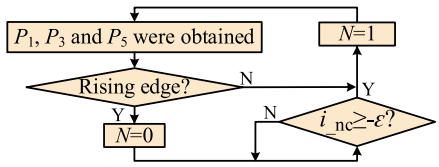

Fig. 7 Determination basis of variable N.

TABLE I
SECTOR ESTIMATION

P_1	P_3	P_5	$F_{\_nc}$	N	Sector estimation
1	0	0	1	1	sector 2
0	1	0	1	1	sector 3
0	0	1	1	1	sector 1

It can be seen from Fig. 6 that $N = 0$ corresponds to the shaded part and $N = 1$ corresponds to the outside of the shaded part. Therefore, under the condition of $N = 1$, fault detection of position sensors can be realized according to $F_{\_nc} = 1$ to avoid the occurrence of misdiagnosis. Besides, when the fluctuation of nonconduction phase current occurs at commutation interval, it will not lead to erroneous diagnosis. The reason is as follows: the fluctuation of the nonconduction phase current will only change the current amplitude. Based on the above analysis, it can be seen that the waveforms of nonconduction phase current under different current amplitudes are similar to Fig. 6 and the only difference is the width of $N = 0$. Therefore, $i_{\_nc} > -\varepsilon$ under $N = 1$ can still be detected, and $F_{\_nc} = 0$ can be detected combined with (7), i.e., it will not lead to erroneous diagnosis.

In summary, the expression of F_{ps} for fault detection of position sensor can be obtained by (2), (7) and the variable N in Fig. 6 as follows:

$$F_{ps} = F_{det} \cup (F_{\_nc} \cap N) \tag{8}$$

where $F_{ps} = 1$ indicates that the position sensor is faulty and $F_{ps} = 0$ indicates that the position sensor is normal.

It should be noted that the sector in which the rotor is located can be estimated by $F_{\_nc} = 1$, $N = 1$ and the driving signal of upper switch, as shown in Table I. For example, when $P_5 = 1$, T_5T_6 works. If $F_{\_nc} = 1 \& N = 1$ is detected, it can be seen that the characteristics appears in the 360°–420° interval of Fig. 4(a) according to the analysis of Fig. 5, and the 360°–420° interval is located in sector 1 according to Fig. 2. Therefore, it can be estimated that the rotor is located in sector 1 by $F_{\_nc} = 1 \& N = 1 \& P_5 = 1$. Besides, according to Fig. 2, the switch operating in sector 1 is T_1T_2, not T_5T_6. Therefore, in order to reduce the time of error commutation, the T_5T_6 should be switched to the T_1T_2 after $F_{\_nc} = 1 \& N = 1 \& P_5 = 1$ was detected. Based on the above, the conducting logic diagram of switch can be

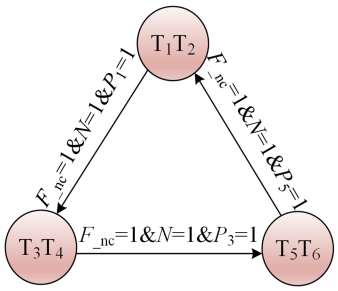

Fig. 8 Conduction logic diagram of switch based on $F_{\_nc}$, N and the driving signal of upper switch.

obtained, as shown in Fig. 8, where the arrows are the switching conditions.

B. Fault Location

Although the fault detection can be achieved by (8), the fault location cannot be achieved. According to the faulty number of position sensors, there are the following three categories: 1) single position sensor fault, 2) two position sensors fault, and 3) three position sensors fault. The following analyzes the characteristics of fault location from the above three categories, respectively.

(i) Single position sensor fault

When single position sensor is faulty, taking position sensor 1 as an example, the following four fault cases can be analyzed according to the analysis of B in Section II.

1) When the low level fault 1 occurs, as shown in Fig. 4(a), where T_5T_6 works in the 360°–420° interval. According to the previous analysis, it can be seen that $F_{\_nc} = 1\&N = 1\&P_5 = 1$ can be detected in the 360°–420° interval, and 360°–420° interval is located in the sector 1 combined with Table I. However, when the position sensor 1 is normal, it can be seen from Fig. 6 that the $F_{\_nc} = 1\&N = 0\&P_1 = 1$ or $F_{\_nc} = 0\&N = 1\&P_1 = 1$ can be detected in the 360°–420° interval of sector 1. Since the characteristics are different before and after the fault, $F_{\_nc} = 1\&N = 1\&P_5 = 1$ detected after the fault can be used as the characteristics of fault location.
2) When the high level fault 1 occurs, as shown in Fig. 4(c). According to $F_{\rm det} = 1$ at 240°, $F_{\rm ps} = 1$ can be obtained by (8). Comparing Figs. 2 and 4(c), it can be seen that: $H_1 = 0$ at 300° (i.e., $H_2\downarrow$) in Fig. 2, while $H_1 = 1$ at 300° in Fig. 4(c). Therefore, the detected $F_{\rm ps} = 1\&H_2\downarrow\&H_1 = 1$ after faults can be used as the characteristics of fault location.
3) When the low level fault 2 occurs, it is categorized into two cases according to the moment of fault occurrence, as shown in Figs. 4(b) and 9.

When the fault occurs in Fig. 4(b), the analysis is similar to 1) and the characteristics of fault location are the same as 1).

When the fault occurs in Fig. 9, according to $H_1\downarrow$, $H_2 = 0$, and $H_3 = 0$ at $\theta_{\rm F}$, $F_{\rm det} = 1$ can be obtained by (2) and $F_{\rm ps} = 1$ can be obtained by (8). Since the rising edge does not appear at $\theta_{\rm F}$, the system is not triggered to commutation, which

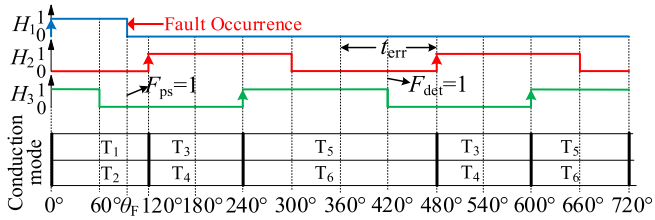

Fig. 9 Low level fault 2 occurs in position sensor 1.

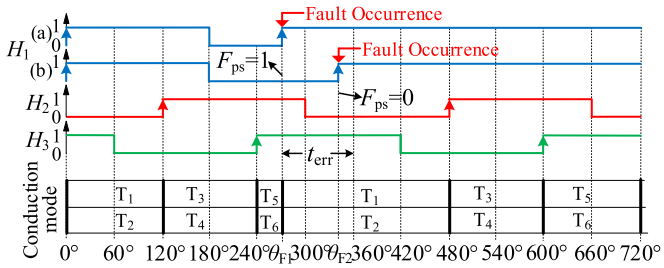

Fig. 10 High level fault 2 occurs in position sensor 1.

makes T_1T_2 continue to work in the $\theta_{\rm F}$∼120° interval. Since T_1T_2 works in both the 60°–120° interval of Fig. 2 and the 60°–120° interval of Fig. 9, the characteristics of phase current in the 60°–120° interval of Fig. 9 are the same as the 60°–120° interval of Fig. 2($i_{\rm a} = -i_{\rm c}$, $i_{\_nc} = i_{\rm b} = 0$), thus, $F_{\_nc} = 0$ can be obtained by (7). Comparing Figs. 3 and 9, it can be seen that $P_1 = 1$, P_3 and P_5 are 0 in the 0°∼120° interval, and $N = 1$ can be obtained by combining with Fig. 7. Therefore, the detected characteristics at $\theta_{\rm F}$ (i.e., $H_1\downarrow$) are $P_1 = 1\&F_{\_nc} = 0\&N = 1$.

When the position sensor 1 is normal, it can be obtained from Fig. 6 that $i_{\_nc} = i_{\rm c} = 0$, $N = 1$, and $P_3 = 1$ at $H_1\downarrow$, and $F_{\_nc} = 0$ can be obtained by (7). Therefore, $P_3 = 1\&F_{\_nc} = 0\&N = 1$ can be detected at $H_1\downarrow$.

In summary, since the characteristics detected at $H_1\downarrow$ before and after the fault are different, $F_{\rm ps} = 1\&P_1 = 1\&F_{\_nc} = 0\&N = 1$ detected at $H_1\downarrow$ after the fault can be used as characteristics of fault location.

4) When the high level fault 2 occurs, it is categorized into three cases according to the moment of fault occurrence, as shown in Figs. 4(d) and 10.

When the fault occurs in Fig. 4(d), according to $F_{\rm det} = 1$ at $\theta_{\rm F}$, $F_{\rm ps} = 1$ can be obtained by (8). Comparing Figs. 2 and 4(d), it can be obtained that: the order of the rising edge in the 120°–240° interval in Fig. 2 is $H_2\uparrow\rightarrow H_3\uparrow$, while the order of the rising edge in the 120°–240° interval in Fig. 4(d) is $H_2\uparrow\rightarrow H_1\uparrow\rightarrow H_3\uparrow$. Therefore, the fault location can be realized by detecting the trigger sequence of $H_{\rm k}$, and the characteristic of fault location is $F_{\rm ps} = 1\&H_2\uparrow\rightarrow H_1\uparrow$. Besides, since T_1T_2 works in the $\theta_{\rm F}$∼240° interval in Fig. 4(d), the system is resulted in erroneous commutation. In order to prevent this phenomenon from occurring, when the characteristic of the fault location is detected, the system does not output the commutation information and keeps the prefault working state, i.e., T_3T_4 still works in the $\theta_{\rm F}$∼240° interval in Fig. 4(d).

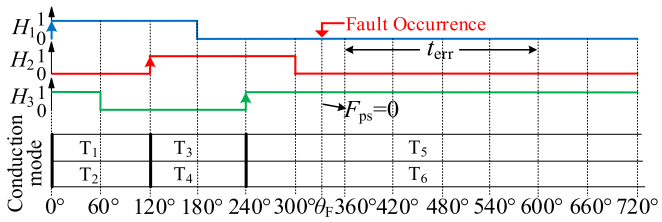

Fig. 11 Fault occurs in three position sensors.

TABLE II
CHARACTERISTICS OF FAULT LOCATION FOR POSITION SENSOR 1

$F_{\_nc}$=1&N=1&P_5=1
F_{ps}=1&P_1=1&$F_{\_nc}$=0&N=1
F_{ps}=1&$H_2\downarrow$&H_1=1
F_{ps}=1&$H_2\uparrow\rightarrow H_1\uparrow$
F_{ps}=1&$H_3\uparrow$&H_1=1
F_{ps}=1&$H_1\downarrow$&$H_2\uparrow$
F_{ps}=1&$H_1\uparrow$&$H_2\downarrow$
F_{ps}=1&$H_1\downarrow$&$H_3\downarrow$
F_{ps}=1&$H_1\uparrow$&$H_3\uparrow$

When the fault occurs in θ_{F1} or θ_{F2} in Fig. 10, the analysis is similar to 2) and the characteristics of fault location are the same as 2).

(ii) Two position sensors fault

When two position sensors are faulty, the analysis is similar to (i) and the fault location characteristics of position sensor 1 can be obtained by F_{ps}, the jumping edge of H_k, $F_{\_nc}$ and the driving signals of upper switch as follows: $F_{\_nc} = 1\&N = 1\&P_5 = 1$, $F_{ps} = 1\&H_3\uparrow\&H_1 = 1$, $F_{ps} = 1\&H_2\downarrow\&H_1 = 1$, $F_{ps} = 1\&H_1\downarrow\&H_2\uparrow$, $F_{ps} = 1\&H_1\uparrow\&H_2\downarrow$, $F_{ps} = 1\&H_1\downarrow\&H_3\downarrow$, and $F_{ps} = 1\&H_1\uparrow\&H_3\uparrow$.

(iii) Three position sensors fault

When the three position sensors are faulty, the analysis is different from (i) or (ii), in which fault location cannot be achieved by the jumping edge of H_k, but only by the nonconduction phase current $i_{\_nc}$. As shown in Fig. 11, H_1 and H_2 are 0, and H_3 is 1 after θ_F. Since the jumping edge of H_k will not be generated after fault, it is difficult to locate the fault based on the jumping edge of H_k. However, according to the previous analysis, it is known that fault location of position sensor can be realized based on the nonconduction phase current $i_{\_nc}$ in one electrical angle period, where the location characteristics of the position sensor 1 in Fig. 11 are the same as 1) of (i).

In summary, the characteristics of fault location of position sensor 1 are summarized, as shown in Table II. Similarly, it can be obtained that the characteristics of fault location for position sensor 2 and position sensor 3 are shown in Table III by adopting the analysis method of position sensor 1 fault.

Based on the above, the fault location flags F_1, F_2, and F_3 of the position sensor 1, position sensor 2, and position sensor 3 are defined as follows:

$$F_1 = \begin{cases} 1 & \text{satisfy Table II} \\ 0 & \text{others} \end{cases} \tag{9}$$

TABLE III
CHARACTERISTICS OF FAULT LOCATION FOR POSITION SENSOR 2 AND POSITION SENSOR 3

Characteristics of fault location for position sensor 2 (COFLFPS2)	Characteristics of fault location for position sensor 3 (COFLFPS3)
$F_{\_nc}$=1&N=1&P_1=1	$F_{\_nc}$=1&N=1&P_3=1
F_{ps}=1&P_3=1&$F_{\_nc}$=0&N=1	F_{ps}=1&P_5=1&$F_{\_nc}$=0&N=1
F_{ps}=1&$H_3\downarrow$&H_2=1	F_{ps}=1&$H_1\downarrow$&H_3=1
F_{ps}=1&$H_3\uparrow\rightarrow H_2\uparrow$	F_{ps}=1&$H_1\uparrow\rightarrow H_3\uparrow$
F_{ps}=1&$H_1\uparrow$&H_2=1	F_{ps}=1&$H_2\uparrow$&H_3=1
F_{ps}=1&$H_2\downarrow$&$H_3\uparrow$	F_{ps}=1&$H_3\downarrow$&$H_1\uparrow$
F_{ps}=1&$H_2\uparrow$&$H_3\downarrow$	F_{ps}=1&$H_3\uparrow$&$H_1\downarrow$
F_{ps}=1&$H_2\downarrow$&$H_1\downarrow$	F_{ps}=1&$H_3\downarrow$&$H_2\downarrow$
F_{ps}=1&$H_2\uparrow$&$H_1\uparrow$	F_{ps}=1&$H_3\uparrow$&$H_2\uparrow$

$$F_2 = \begin{cases} 1 & \text{satisfy COFLFPS2 of Table III} \\ 0 & \text{others} \end{cases} \tag{10}$$

$$F_3 = \begin{cases} 1 & \text{satisfy COFLFPS3 of Table III} \\ 0 & \text{others} \end{cases} \tag{11}$$

where $F_1 = 1$ indicates that position sensor 1 is faulty, and $F_1 = 0$ indicates that position sensor 1 is normal. F_2 and F_3 are defined similarly to F_1. According to (9)–(11), the fault location table of position sensors can be obtained, as shown in Table VI.

C. Fault-Tolerant Control

After fault location of position sensor is completed, the erroneous position signal should be turned off to ensure fault-tolerant operation.

When the motor is running normally, the count values between the adjacent rising edges of the position signal are captured by the DSP and averaged to obtain the speed and position angle of motor, as shown in

$$n = 60/(p_r z T_p); z = \sum_{k=1}^{3}(y_k z_k)/\left(\sum_{k=1}^{3} y_k\right) \tag{12}$$

$$\theta_k = \theta_{k\_up} + p_r \omega t \frac{180}{\pi} = \theta_{k\_up} + p_r t \frac{180}{\pi}\frac{2\pi n}{60}$$
$$= \theta_{k\_up} + 6 p_r n t \tag{13}$$

where n is the speed of the motor and p_r is the number of rotor poles of DSEM. z is the average value between the adjacent rising edges of the three position signals. T_p is the period of DSP counter. z_k is the calculated value between the adjacent rising edges of the position sensor k. y_k is the fault flag coefficient, and $y_k = 1$ when position sensor k is normal. θ_k is the rotor position angle calculated by the position sensor k. It can be found that θ_1, θ_2, and θ_3 differ from each other by 120° in turn, which means that as long as the angle of any one of θ_1, θ_2, and θ_3 is obtained, the position angles of the other two can be obtained by the relationship between each other, which provides a channel for the subsequent fault-tolerant control. θ_{k_up} is the rotor position angle at the rising edge of H_k.

When one or two position sensors are faulty, the count values between adjacent rising edges of the remaining normal position

TABLE IV
FAULT LOCATION TABLE OF POSITION SENSORS

F_1	F_2	F_3	Faulty sensor
1	0	0	Position sensor 1
0	1	0	Position sensor 2
0	0	1	Position sensor 3
1	1	0	Position sensor 1 and position sensor 2
1	0	1	Position sensor 1 and position sensor 3
0	1	1	Position sensor 2 and position sensor 3
1	1	1	Three position sensors

TABLE V
FAULT-TOLERANT STRATEGY TABLE

Faulty sensor	Fault-tolerant strategy
Position sensor 1	y_1=0, y_2=y_3=1; k=2 or 3 in (13)
Position sensor 2	y_2=0, y_1=y_3=1; k=1 or 3 in (13)
Position sensor 3	y_3=0, y_1=y_2=1; k=1 or 2 in (13)
Position sensor 1 and position sensor 2	y_1=y_2=0, y_3=1; k=3 in (13)
Position sensor 1 and position sensor 3	y_1=y_3=0, y_2=1; k=2 in (13)
Position sensor 2 and position sensor 3	y_2=y_3=0, y_1=1; k=1 in (13)
Three position sensors	Position sensorless control

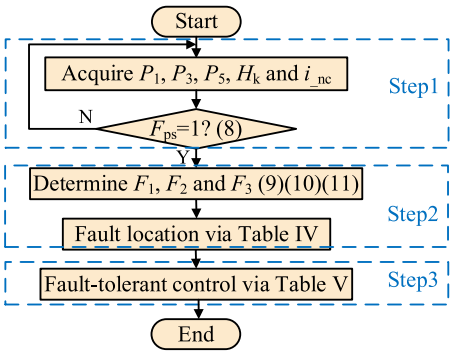

Fig. 12 Fault diagnosis flowchart of the proposed method.

signals are captured by the DSP and averaged to obtain the speed and position angle. For example, when the position sensor 1 fault is located, the n can be obtained by making $y_1 = 0$ and $y_2 = y_3 = 1$ in (12). Due to the position sensor 1 fault, it is difficult to obtain θ_{1_up} and θ_1. However, it can be known from the previous analysis that θ_2 or θ_3 can be obtained by (13), and then θ_1 can be obtained according to the symmetry. When three position sensors are faulty, fault-tolerant control can only be achieved by position sensorless control, which is beyond the scope of this article. In summary, fault-tolerant strategy table for position sensor can be obtained, as shown in Table V.

Fig. 12 shows the fault diagnosis flowchart of the proposed method, which is divided into three steps below.

Step1: Sampling the driving signal of the upper switch (P_1, P_3, P_5), the position signal H_k (H_1, H_2, H_3), the nonconduction phase current $i_{\_nc}$, and the fault detection is realized according to (8).

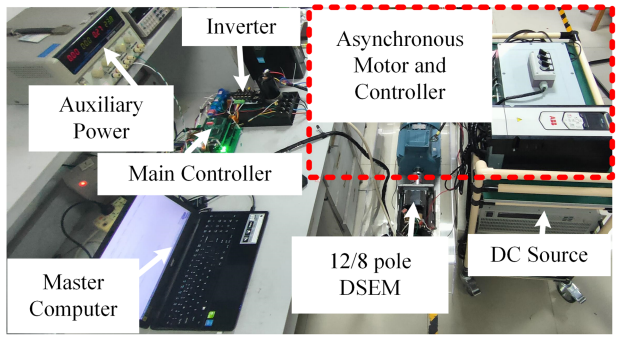

Fig. 13 Experimental platform.

TABLE VI
EXPERIMENTAL CONDITIONS

Parameter	Value	Parameter	Value	Parameter	Value
Motor type	12/8-pole	U_{dc}	150 V	f_T	10 kHz
L_{pmax}/L_{pmin}	2/0.4 mH	n	1000 r/min	T_s	25 μs
L_{pfmax}/L_{pfmin}	15/2.8 mH	i_f	5 A	ε	0.3 A

Step2: Determining F_1, F_2, and F_3 in (9)–(11), and the fault location is realized according to Table IV.

Step3: Realizing the fault-tolerant control according to Table V.

IV. EXPERIMENTAL RESULTS

To verify the effectiveness of the proposed fault diagnosis method, fault experiments of position sensor are carried out on DSEM drive system. Fig. 13 shows the experimental platform of DSEM drive system, which includes DSEM, a coaxially connected induction motor as a load machine, bridge converter, dc power supply, and main controller. The experimental conditions are shown in Table VI, where f_T indicates switching frequency. Besides, the hall current sensor CSM050B with the accuracy of 0.5% was used in the experiment to accurately acquire the current. Meanwhile, in order to prevent the effects of external interference, noise and ripple at the source, differential circuits are used in the experiments in order to sample accurate current information, especially for small currents.

A. Steady Experiments

1) Fault of Single Position Sensor: Since the fault diagnosis process of the three hall position sensors is the same, the following takes the fault of position sensor 1 as an example for experimental verification.

Figs. 14 –17 show the position signal H_k, the driving signals of the upper switch (P_1, P_3, P_5), the phase current i_p, N, F_{ps}, the fault location flags (F_1, F_2, F_3), and n for the four fault states of the position sensor 1 under steady conditions, where n and load are set to 1000 r/min and 3 N·m, respectively.

Fig. 14 shows the experimental results of position sensor 1 with low level fault 1, where the moment of fault occurrence for Fig. 14(a) is consistent with Fig. 4(a) and the moment of fault occurrence in Fig. 14(b) is in the commutation interval. First, it

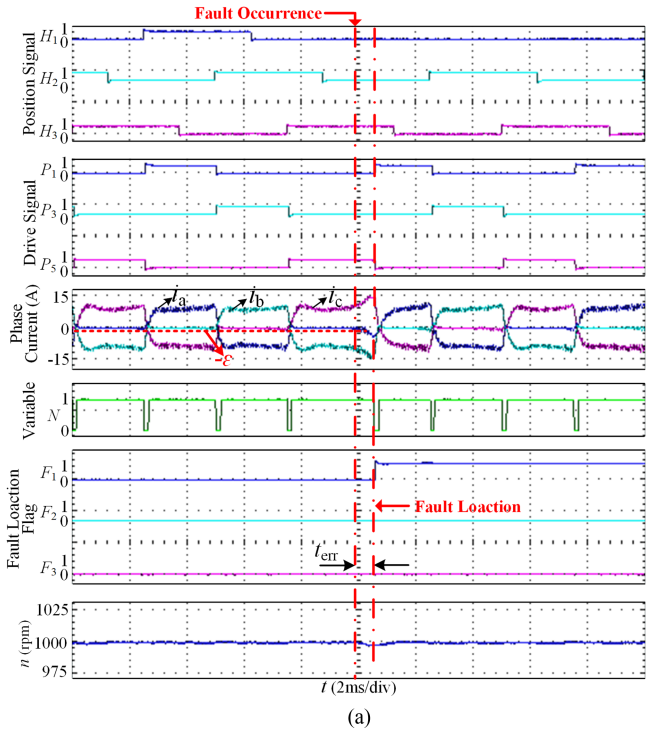

Fig. 14 Experimental results of position sensor 1 with low level fault 1. (a) Fault occurs in the non-commutation interval. (b) Fault occurs in the commutation interval.

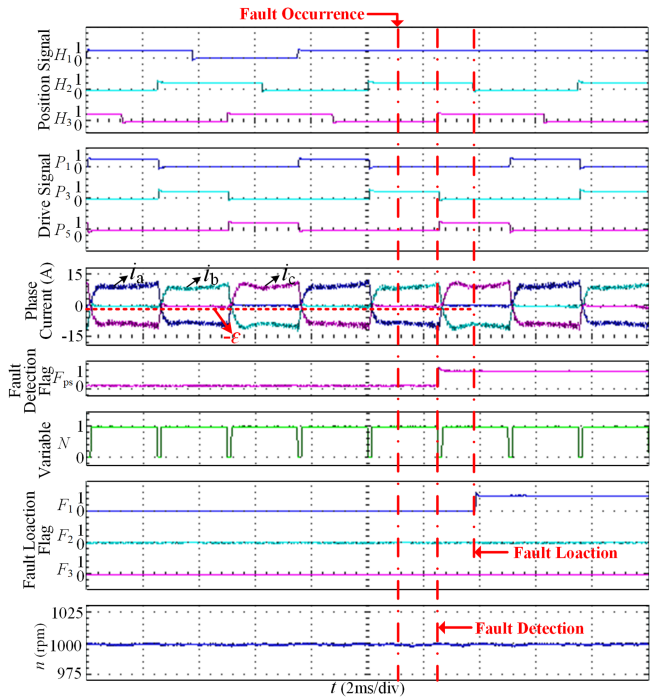

Fig. 15 Experimental results of position sensor 1 with high level fault 1.

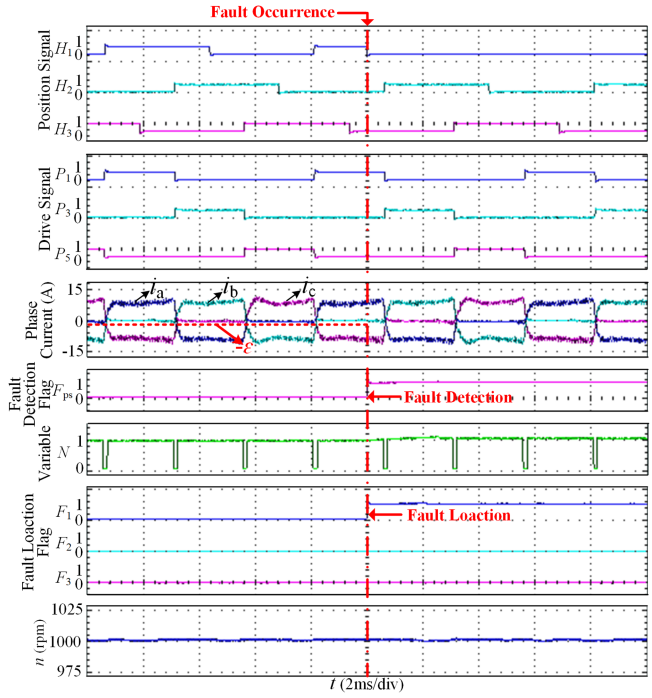

Fig. 16 Experimental results of position sensor 1 with low level fault 2.

can be found that $P_5 = 1$ between the two red dashed lines in the figure, and the nonconduction phase current is i_a by combining Fig. 2 and Fig. 3. Second, according to $i_a < -\varepsilon$ at the right red dashed line, $F\_{nc} = 1$ can be obtained by (7). At the same time, $F\_{nc} = 1 \& N = 1 \& P_5 = 1$ can be obtained combining with $N = 1$ and $P_5 = 1$ at the right red dashed line, which means that it can satisfy the location characteristics of position sensor 1 in Table II. Finally, $F_1 = 1$ can be obtained by (9). Besides, the slight fluctuation of n within the t_{err} time period is caused by the erroneous commutation of the system.

Based on the experimental results in Fig. 14, it can be seen that the proposed method is not influenced by the moment of fault occurrence.

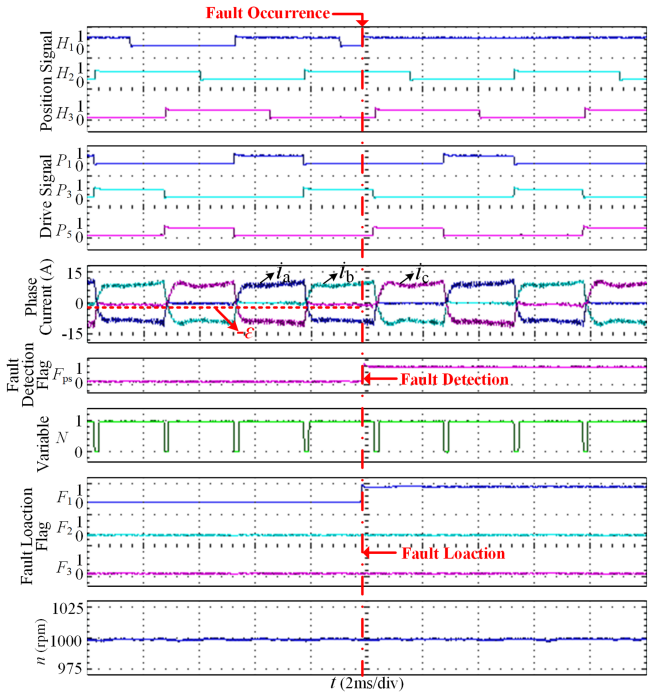

Fig. 17 Experimental results of position sensor 1 with high level fault 2.

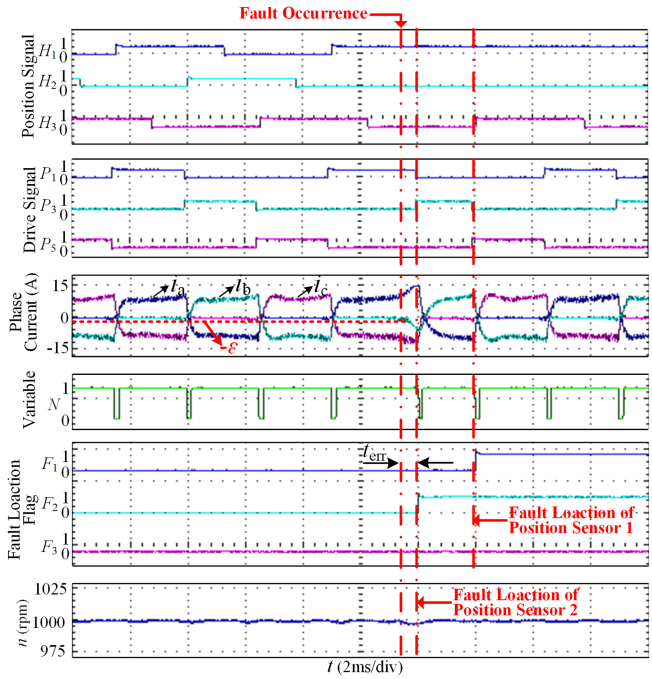

Fig. 18 Experimental results for position sensor 1 with high level fault 1 and position sensor 2 with low level fault 1.

Fig. 15 shows the experimental results of position sensor 1 with high level fault 1, where the fault occurrence moment is consistent with Fig. 4(c). It can be seen that $H_1 = H_2 = 1$, and $H_3\uparrow$ at the second red dashed line after the fault occurs, and $F_{\rm ps} = 1$ can be obtained by (2) and (8). $H_1 = 1$ is detected at the falling edge of H_2 (the third red dashed line in the figure), which satisfies the location characteristics of position sensor 1 in Table II: $F_{\rm ps} = 1\&H_2\downarrow\&H_1 = 1$, and $F_1 = 1$ can be obtained by (9).

When the low level fault 2 occurs in position sensor 1, according to analysis of *B* in Section III, it can be divided into two cases: The first case is that the fault occurs in Fig. 4(b), and the fault diagnosis process is similar to Fig. 14. The second case is that the fault occurs in 0°–120° interval, as shown in Fig. 16. First, due to $P_1 = 1$ at the red dashed line, the nonconduction phase current is $i_{\rm b}$ by combining with Figs. 2 and 3. Second, according to $i_{\rm b} > -\varepsilon$ at the red dashed line, $F_{\_{\rm nc}} = 0$ can be obtained by (7). At the same time, $F_{\rm ps} = 1\&P_1 = 1\&F_{\_{\rm nc}} = 0\&N = 1$ can be obtained combining with $N = 1$ and $F_{\rm ps} = 1$ at the red dashed line, which means that it can satisfy the location characteristics of position sensor 1 in Table II. Finally, $F_1 = 1$ can be obtained by (9).

When the high level fault 2 occurs in position sensor 1, according to analysis of *B* in Section III, it is divided into three cases: The first case is that the fault occurs in Fig. 4(d), as shown in Fig. 17. First, according to $H_1\uparrow$, $H_2 = 1$, and $H_3 = 0$ at the red dashed line, $F_{\rm ps} = 1$ can be obtained by (2) and (8). Second, combined with the rising edge of position signal before the fault is $H_2\uparrow$, the order of the rising edge for position signal is obtained as $H_2\uparrow\rightarrow H_1\uparrow$, which meets the location characteristics of the position sensor 1 in Table II: $F_{\rm ps} = 1\&H_2\uparrow\rightarrow H_1\uparrow$. Finally, $F_1 = 1$ can be obtained by (9). The other two cases for the fault occurs in Fig. 10, where the fault diagnostic process is similar to Fig. 15.

2) Fault of Two Position Sensors: When two position sensors are faulty, fault location is still realized by the nonconduction phase current and position signals. The following experimental verification is carried out by taking the fault of position sensor 1 and the fault of position sensor 2 as an example.

Fig. 18 shows the experimental results for position sensor 1 with high level fault 1 and position sensor 2 with low level fault 1, where *n* and load are set to 1000 r/min and 3 N·m, respectively. According to the characteristics of nonconduction phase current $i_{\rm b} < -\varepsilon$ at the second red dashed line, the fault of position sensor 2 can be localized, and the fault of position sensor 1 can also be localized according to $H_1 = 1$ of $H_3\uparrow$ at the third red dashed line.

3) Fault of Three Position Sensors: When the three position sensors are faulty, fault location can only be achieved by nonconduction phase currents, and the fault diagnosis process is similar to the fault diagnosis of Fig. 14 or the fault diagnosis of position sensor 2 in Fig. 18.

B. Dynamic Experiments

In order to verify the effectiveness of the proposed method under dynamic conditions, fault diagnosis experiments of position sensors under four conditions such as acceleration, deceleration, loading, and load reduction are carried out. Considering that proposed method realizes fault diagnosis based on $H_{\rm k}$ and nonconduction phase current $i_{\_{\rm nc}}$, where the $H_{\rm k}$ is unaffected by variation of speed or load, while the $i_{\_{\rm nc}}$ will vary with variation

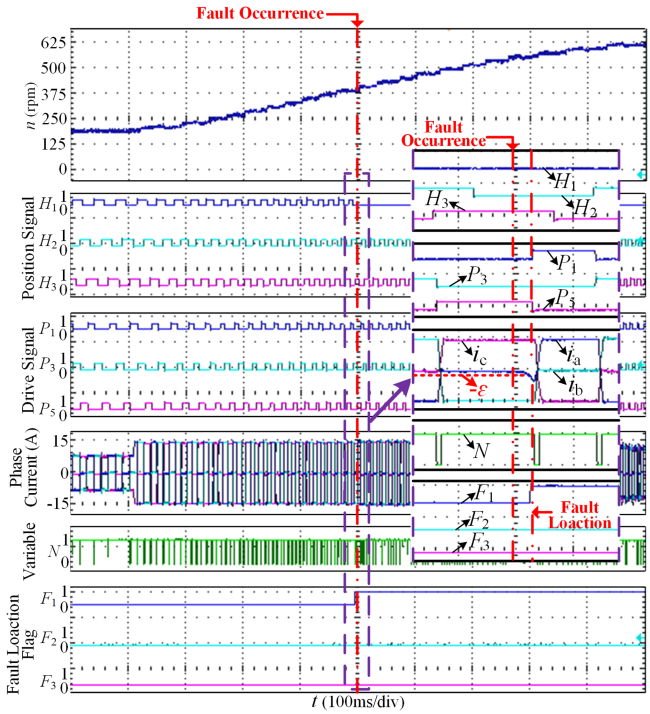

Fig. 19 Experimental results for position sensor 1 with low level fault 1 during acceleration.

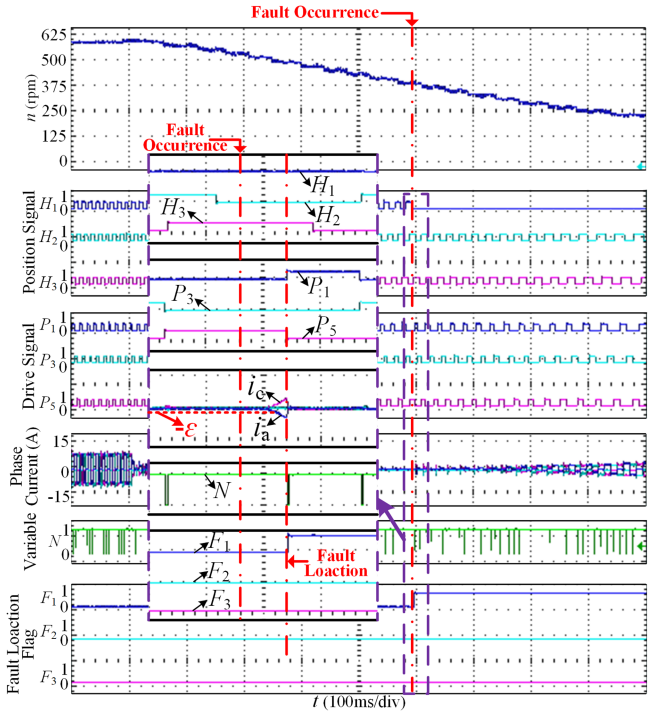

Fig. 20 Experimental results for position sensor 1 with low level fault 1 during deceleration.

of load or speed, thus, the following verifies the validity of the fault diagnosis based on the nonconduction phase current under dynamic conditions (taking position sensor 1 with a low level fault 1 as an example).

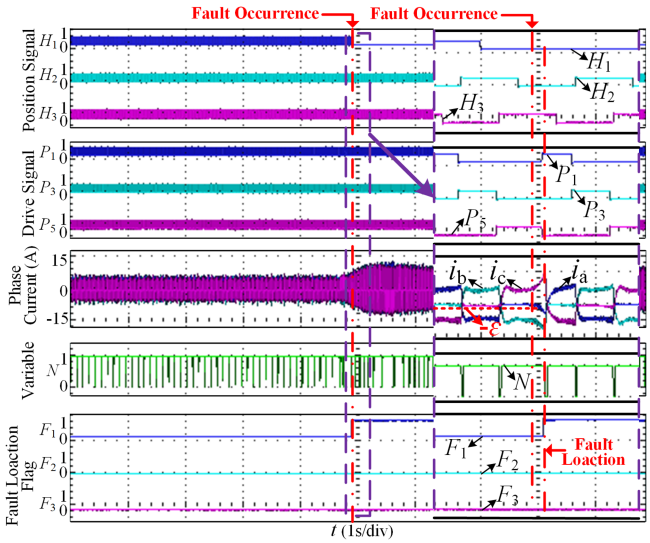

Fig. 21 Experimental results for position sensor 1 with low level fault 1 during loading.

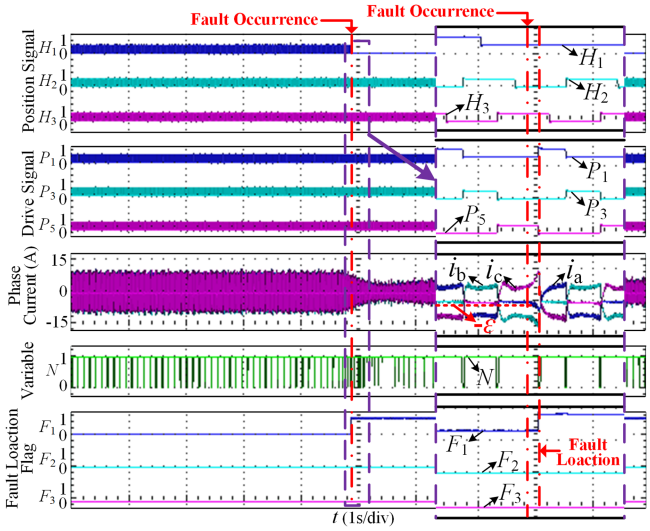

Fig. 22 Experimental results for position sensor 1 with low level fault 1 during load reduction.

Figs. 19–22 show the experimental results of position sensor 1 with a low-level fault 1 during acceleration, deceleration, loading, and load reduction, where the purple arrows point to the enlarged view of the dashed box (enlarged only in the time axis). According to the enlarged view of the dashed box, it can be seen that fault location can also still be realized under dynamic conditions based on the characteristics of $i_{\_nc} = i_a < -\varepsilon$ at the second red dashed line.

C. Construction of Actual Rotor Position Angle Under Fault-Tolerant Operation

In order to verify effectiveness of fault-tolerant operation, experiments were carried out on the fault of single position sensor and the fault of two position sensors, where the fault

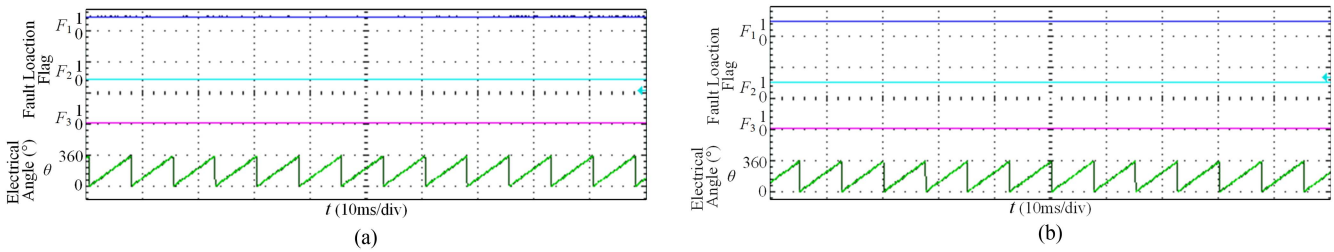

Fig. 23 Fault-tolerant experimental results for position sensor. (a) Position sensor 1 fault. (b) Both position sensor 1 and position sensor 2 fault.

TABLE VII
COMPARISON OF THE PROPOSED METHOD WITH THE EXISTING FAULT DIAGNOSIS METHODS

Fault diagnosis method	Additional detection device	Diagnostic scope	Maximum time of error commutation	Suitable for dynamic conditions	Algorithmic complexity
[12]	Not required	Single	$T_c/3$	No	Complicated
[13]-[15]	Not required	Single	$T_c/3$	No	Complicated
[16]	Not required	Single, two and three	$<T_c/3$	No	Complicated
[17]	Three position sensors	Single, two and three	$<T_c/3$	Yes	Easy
[18]	Not required	Single and two	$<T_c/3$	No	Complicated
[19]	Not required	Single	$T_c/3$	Yes	Easy
Proposed method	Not required	Single, two and three	$<T_c/3$	Yes	Easy

of single position sensor is exemplified by position sensor 1 fault, as shown in Fig. 23(a), the fault of two position sensors are exemplified by the fault of position sensor 1 and the fault of position sensor 2, as shown in Fig. 23(b). It can be found from Fig. 23 that the actual rotor position angle θ can be constructed under fault-tolerant control.

V CONCLUSION

In this article, according to the different performances after the faults of single or two position sensors, fault location is realized through the position signal H_k and nonconduction phase current $i_{\_nc}$ under chopping lower switch control. The fault location of three position sensors is realized by combining the variation characteristics of nonconduction phase current $i_{\_nc}$ under chopping lower switch control in an electrical angle period. Based on sufficient theoretical analysis and experiments, a comparison of the proposed method with the existing fault diagnosis methods of position sensors are listed in Table VII, where T_c is an electrical angle period, which demonstrates that the main contributions of the proposed methods are as follows.

1) Compared with the existing methods, only [16], [17] and the proposed method can realize the fault diagnosis of three position sensors, but only the method proposed in this article both does not require additional detection device and can be applied to dynamic conditions, which helps to reduce the system cost and broaden the application scope of the diagnosis method.
2) A method based on the nonconduction phase current is proposed to realize fault detection and location of the position sensor, which can reduce the time of error commutation and make the maximum time of error commutation less than 1/3 of the electrical angle period, which is conducive to timely switching of fault-tolerant strategies and minimizing the damage of faults to the system.
3) The proposed method is easy to be implemented in a low-cost controller, and the algorithm is simple without using additional hardware and complex modeling process. The inputs are only the driving signal of upper switch, position signal, and nonconduction phase current under chopping lower switch control. The outputs are the fault position.
4) For motors with small no-load currents, if the no-load current is less than the maximum value of sampling error when $i_p = 0$, it is difficult to determine the current threshold because the design of the current threshold cannot satisfy the two requirements of preventing misdiagnosis and preventing missed diagnosis at the same time.
5) The proposed method cannot be applied to permanent magnet synchronous motor due to the three-phase windings work at the same time and there is no nonconduction phase current.

REFERENCES

[1] Y. Wang, Z. Zhang, R. Liang, W. Yuan, and Y. Yan, "Torque density improvement of doubly salient electromagnetic machine with asymmetric current control," *IEEE Trans. Ind. Electron.*, vol. 63, no. 12, pp. 7434–7443, Dec. 2016.
[2] W. Jia and L. Xiao, "Research on control strategies for doubly salient electromagnetic machine," *IET Electr. Power Appl.*, vol. 11, no. 8, pp. 1449–1456, Sep. 2017.
[3] M. A. Elgendy, V. Pickert, B. Zahawi, C. Morton, and A. Ayob, "Dual voltage supply converter for high-speed doubly salient reluctance motors," *IEEE Trans. Power Electron.*, vol. 28, no. 2, pp. 1016–1024, Feb. 2013.
[4] J. Wei, T. Zhang, P. Liu, W. Tao, and B. Zhou, "Investigation of a fault-tolerant control method for a multiport dual-stator doubly salient electromagnetic machine drive," *IEEE Trans. Ind. Electron.*, vol. 66, no. 1, pp. 750–761, Jan. 2019.

[5] S. Jiang, B. Zhou, X. Huang, L. Xiong, J. Wei, and K. Zhou, "Fault-tolerant system design for doubly salient electromagnetic machine under loss of excitation," *IEEE Trans. Power Electron.*, vol. 37, no. 4, pp. 4589–4599, Apr. 2022.
[6] L. Dong, J. Jatskevich, Y. Huang, M. Chapariha, and J. Liu, "Fault diagnosis and signal reconstruction of hall sensors in brushless permanent magnet motor drives," *IEEE Trans. Energy Convers.*, vol. 31, no. 1, pp. 118–131, Mar. 2016.
[7] M. Ebadpour, N. Amiri, and J. Jatskevich, "Fast fault-tolerant control for improved dynamic performance of hall-sensor-controlled brushless DC motor drives," *IEEE Trans. Power Electron.*, vol. 36, no. 12, pp. 14051–14061, Dec. 2021.
[8] L. Dong, Y. Huang, J. Jatskevich, and J. Liu, "Improved fault-tolerant control for brushless permanent magnet motor drives with defective hall sensors," *IEEE Trans. Energy Convers.*, vol. 31, no. 2, pp. 789–799, Jun. 2016.
[9] Y. Zhao, W. Huang, and J. Yang, "Fault diagnosis of low-cost hall-effect sensors used in controlling permanent magnet synchronous motor," in *Proc. IEEE 19th Int. Conf. Elect. Mach. Syst.*, 2016, pp. 1–5.
[10] E. Balaban, A. Saxena, P. Bansal, K. Goebel, and S. Curran, "Modeling, detection, and disambiguation of sensor faults for aerospace applications," *IEEE Sensors J.*, vol. 9, no. 12, pp. 1907–1917, Dec. 2009.
[11] P. Alaeinovin and J. Jatskevich, "Filtering of hall-sensor signals for improved operation of brushless DC motors," *IEEE Trans. Energy Convers.*, vol. 27, no. 2, pp. 547–549, Jun. 2012.
[12] C. Ma and B. Zhou, "Fault diagnosis and fault-tolerant control of position signal for doubly salient motor," *Proc. CSEE*, vol. 28, no. 18, pp. 73–78, Jun. 2008.
[13] P. Xu et al., "Fault diagnosis and fault-tolerant control of position signals for switched reluctance motors," *Proc. CSEE*, vol. 31, no. 33, pp. 123–130, Nov. 2011.
[14] H. Chen, G. Guan, G. Han, and H. Chen, "Fault diagnosis and tolerant control strategy for position sensors of switched reluctance starter/generator systems," *IEEE Trans. Transport. Electrific.*, vol. 6, no. 4, pp. 1508–1518, Dec. 2020.
[15] J. Cai and X. Zhao, "Synthetic hybrid-integral-threshold logic-based position fault diagnosis scheme for SRM drives," *IEEE Trans. Instrum. Meas.*, vol. 70, pp. 1–8, Oct. 2021.
[16] R. Hu, Z. Deng, J. Cai, and C. Wang, "A fault diagnosis and fault-tolerant control method for position signal of switched reluctance motor," *Trans. China Electrotechnical Soc.*, vol. 29, no. 7, pp. 104–113, Jul. 2014.
[17] M. Aqil and J. Hur, "A direct redundancy approach to fault-tolerant control of BLDC motor with a damaged hall-effect sensor," *IEEE Trans. Power Electron.*, vol. 35, no. 2, pp. 1732–1741, Feb. 2020.
[18] Q. Zhang and M. Feng, "Fast fault diagnosis method for hall sensors in brushless DC motor drives," *IEEE Trans. Power Electron.*, vol. 34, no. 3, pp. 2585–2596, Mar. 2019.
[19] A. Mousmi, A. Abbou, and Y. El Houm, "Binary diagnosis of hall effect sensors in brushless DC motor drives," *IEEE Trans. Power Electron.*, vol. 35, no. 4, pp. 3859–3868, Apr. 2020.
[20] X. Zhou et al., "Online adaptive maximum torque per ampere control for doubly salient electromagnetic machine," *IEEE Trans. Energy Convers.*, vol. 38, no. 4, pp. 2811–2821, Dec. 2023.
[21] C. Hu, B. Zhou, and J. Wei, "On line diagnosis of single tube open circuit fault in full bridge converter of doubly salient motor," *Proc. CSEE.*, vol. 29, no. 33, pp. 111–116, Nov. 2009.

Yijun Zhang was born in Xinyang, China, in 1996. He received the B.S. degree in electrical engineering from Zhengzhou University of Light Industry, Zhengzhou, China, in 2019, and the M.S. degree in electrical engineering in 2022 from Nanjing University of Aeronautics and Astronautics, Nanjing, China, where he is currently working toward the Ph.D. degree in power electronics and drives.

His research interest includes fault diagnosis technology in Brushless dc motor drive system.

Bo Zhou was born in Wenzhou, China, in 1961. He received the B.S. degree in electrical engineering from Zhejiang University, Hangzhou, China, in 1983, the M.S. degree in control engineering from Chongqing University, Chongqing, China, in 1986, and the Ph.D. degree in electrical engineering from Nanjing University of Aeronautics and Astronautics (NUAA), Nanjing, China, in 2000.

He is currently a Professor with the College of Automation Engineering, NUAA, and is the Director with the Jiangsu Key Laboratory of New Energy Generation and Power Conversion. His research interests include power converter, electrical machine driving systems, and renewable power systems.

Dr. Zhou was the recipient of the State Technological Invention second-class award in 2009, the Geneva International Invention gold award in 2011, and the Defense Technological Invention first prize in 2008.

Wenjing Fang was born in Weifang, China, in 1995. She received the M.S. degree in control engineering from University of Jinan, Jinan, China, in 2020. She is currently working toward the Ph.D. degree in electrical engineering from Nanjing University of Aeronautics and Astronautics (NUAA), Nanjing, China.

Her research interests include electrical machine driving systems and their applications in aerospace power systems.

Yi Lu was born in Suqian, China, in 1994. He received the B.S. degree in measurement and control technology and instrumentation from Xi'an University of Technology, Shanxi, China, in 2016, the M.S. degree in electrical engineering from Nanjing Institute of Technology, Nanjing, China, in 2021. He is currently working toward the Ph.D. degree in electrical engineering with the Department of Electrical Engineering, Nanjing University of Aeronautics and Astronautics(NUAA), Nanjing, China.

His research interests include the Electrolytic capacitor-less technology in motor drive and power generation systems.

Siyuan Jiang was born in Jiaozuo, China, in 1992. He received the B.S. degree from Chongqing Jiaotong University, Chongqing, China, in 2014, the M.S. degree from Henan Polytechnic University, Jiaozuo, China, in 2018, and the Ph.D. degree from Nanjing University of Aeronautics and Astronautics, Nanjing, China, in 2022, all in electrical engineering. He is currently a Lecturer with the School of Electrical Engineering and Automation, Henan Polytechnic University, Jiaozuo, China. His research interests include design and control technology of special motor.